Synthesis of Metal Oxide Thin Films by Reactive Magnetron Sputtering in Ar/O₂ Mixtures: An Experimental Study of the Chemical Mechanisms

Rony Snyders,* Jean-Pierre Dauchot, Michel Hecq

One of the major limitations of reactive magnetron sputtering (RMS) is the low deposition rate when the target is poisoned. With the goal of reducing this phenomenon, we studied the chemical mechanisms involved during conventional and ionized reactive magnetron sputtering (iRMS) of metals (Sn, Ti, Ag) in Ar/O₂ mixtures. Target surface, plasma and film compositions were characterized by target voltage, MS and XPS measurements, respectively. Comparing films and plasma compositions, we demonstrated that oxide film formation proceeds by condensation of sputtered material and reaction between the growing film and the reactive species, especially O. Using iRMS, we promoted the latter process: for example, we prepared fully oxidized Sn films using low O₂ flows which limits target poisoning and, in turn, increases the deposition rate (6 times).
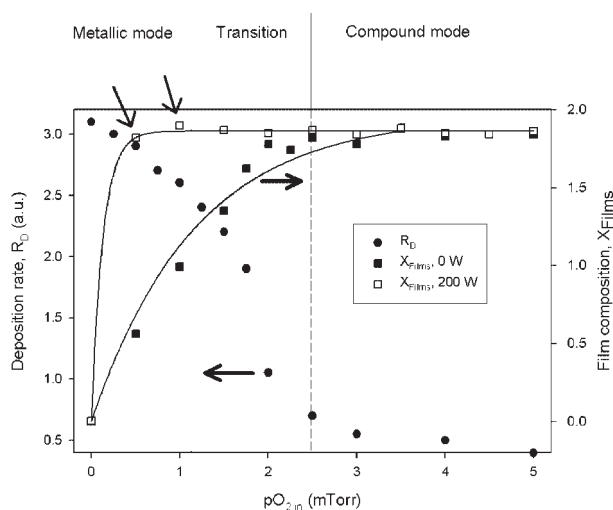
Introduction

Reactive magnetron sputtering (RMS) has been employed for decades for deposition of thin compound films because of its high versatility, good film quality and diverse fields of industrial applications such as decorative,[1] biomedical,[2] optical[3] or architectural glasses.[4] RMS relies on the principle of compound formation by chemical reaction between the sputtered material, a metal, and a reactive gas

R. Snyders, J.-P. Dauchot, M. Hecq
Laboratoire de Chimie Inorganique et Analytique, Université de Mons-Hainaut, Bât. Materia Nova, Parc Initialis, Avenue Copernic, 1, 7000 Mons, Belgium.
E-mail: rony.snyders@umh.ac.be

(R: O₂, N₂, CH₄, . . .) added to the sputtering gas, generally, Ar.[5] In this text, RMS of metal M in Ar/R mixtures will be referred as M-Ar/R.

At first sight, RMS seems a simple process but, in reality, it is quite difficult to control mainly because, during the process, the reactive gas reacts not only with sputtered material to form the compound on the substrate (or on the walls) but also with the target surface. The chemical composition of the latter (X_{Target}) is modified, leading to so-called target poisoning.[6] This effect is responsible for the main technological limitations of RMS namely arcs formation (if the compound formed on the target is electrically insulating) and, above all, a significant decrease of the deposition rate (R_D).[6] These phenomena affect both the quality and production yield of the film.[6]

To overcome these problems and to get a better understanding of RMS, numerous authors, since the early seventies, have proposed models. As examples, Heller et al.[7] and Abe et al.[8] have published qualitative models for Mo,Ti-Ar/O_2 and Mo,Ti-Ar/N_2 discharges. Later, Eltoukhy et al.[9] have introduced in the Abe's model, variations of the secondary electron emission coefficient (γ) as a function of X_{Target} for In-Ar/O_2 and In-Ar/N_2 while Lamperière et al. have taken into account the getter effect of the deposited metal.[10]

Although these models gave reliable results, they focused mainly on the target behavior omitting the role of the chamber walls, the plasma or the substrate. Moreover, they were not convenient due to the difficulty to achieve input parameters such as reactive gas adsorption kinetic and the secondary electron emission coefficient.

In 1987, Berg et al. published a model with simple concepts and low number of parameters.[11] The core idea was to establish mass balance equations for reactive gas and compound including adsorption and sputtering mechanisms on target, walls and substrate. Deposition rate (R_D), partial pressure of reactive gas (p_R) and films composition (X_{Films}) are then calculated as a function of the inflow rate of reactive gas (Φ_R). Despite its simplicity, the response of this model proved to fit well with experimental results. Nevertheless, in certain situations, Berg's model presents some limitations mainly because it does not integrate the plasma chemistry.

The latter was included in Berg's model by Erschov et al.[12] Using Si-Ar/O_2 as model system, the authors theoretically showed the major role of atomic oxygen (O) in the compound formation. The significant role of O in RMS process is now commonly accepted[11–14] but, to our knowledge, no experimental work clearly demonstrates this theoretical prediction.

In order to validate experimentally the latter, we have decided to tune the O density during the RMS process by increasing the discharge reactivity. This goal is reached by coupling, to the conventional RMS, a second plasma generated by a radio-frequency (RF) coil located between the target and the substrate. This coupling increases both the density (n_e) and the temperature (T_e) of the electrons. For such a kind of discharges, n_e ranges between 10^{11} and 10^{13} cm^{-3}, that is about 3 orders of magnitude higher than for conventional RMS.[15–17]

The first consequence of the modification of electron characteristics is the increase of the ionization rate of sputtered metallic species. Consequently, this process will be referred as "ionized reactive magnetron sputtering" (iRMS) in the rest of the text. Actually, the metal ionization level in this discharge can reach at least 20%,[15,18,19] while for conventional systems it is only a few percents.[18] Indeed, due to the increase of n_e and T_e, metal ionization no longer occurs mainly by Penning effect [Equation (1)], but

also by electronic collisions [Equation (2)]:[19,20]

$$Ar^* + M \rightarrow Ar + M^+ + e^- \tag{1}$$

$$M + e^- \rightarrow M^+ + 2e^- \tag{2}$$

In these equations, Ar* is a metastable Ar atom, e$^-$ an electron and M a metal atom. The increase of ionization rate is remarkable, above all, for metallic species because of their low ionization thresholds (Table 1). For sputter gas particles, such as Ar (15.76 eV), O (13.55 eV) and O_2 (12.15 eV) for which the ionization threshold is higher, the effect is weaker. Another important consequence of higher n_e and T_e is the increase of reactive gas dissociation producing higher density of atomic reactive species. This effect has been observed for deposition of alumina using O_2 as reactive gas[23] as well as for deposition of TiN.[24–26] In the latter case, the authors have measured a dissociation level of N_2 ranging from 10–30% depending on the power applied to the external RF coil.[24–26] In the rest of the text, the set of effects related to the use of the RF coil generated secondary plasma will be labeled as "plasma amplification".

In this work, we compare RMS of several metals differing by their reactivity to O_2 (ξ_M) in conventional and iRMS processes. The energy of the M–O bond reported in Table 1 is taken as a measurement of ξ_M. The chemical compositions of the target surface (X_{Target}), the plasma (X_{Plasma}) and the film (X_{Films}) versus O_2 flow are evaluated by both target voltage (V_D) and the deposition rate (R_D), MS and X-ray photoelectron spectroscopy (XPS) measurements, respectively.

The goals of this paper are: (i) to highlight the fundamental chemical mechanisms of RMS at the target,

Table 1. Physico-chemical constants (Energy of M–O bond and first ionization threshold) of the metals and experimental parameters used during experiments (target current, I_D, target current density, I_d, discharge pressure, p_{tot}, fraction of O_2 in the gas mixture, f_{O_2}, total inflow rate of gases, Φ_{Tot} and RF power applied to the coil, P_{RF}).

Property	Sn	Ti	Ag	Ref.
Energy of M–O bond/eV	5.7	7.3	2.4	[20]
First ionization threshold/eV	6.82	7.34	7.58	[21]
I_D/mA	100	350	95	
I_d/mA $\cdot$ cm^{-2}	1.8	6.3	1.7	
p_{tot}/mTorr	5	8	5	
f_{O_2}/%	0 → 100	0 → 25	0 → 100	
Φ_{Tot}/sccm	20	80	20	
P_{RF}/W		0, 100, 200		

Synthesis of Metal Oxide Thin Films by Reactive Magnetron Sputtering in Ar/O$_2$ Mixtures: . . .

Plasma Processes
and Polymers

in the plasma and on the substrate, (ii) to experimentally demonstrate the role of O in RMS processes and (iii) using information deduced from points (i) and (ii), to optimize RMS of metal in Ar/O$_2$ mixtures.

Reactive Sputtering: Theoretical Concepts

As soon as reactive gas is introduced into the sputtering process, it reacts with the target surface and the growing film. Increasing the inflow rate of reactive gas R, Φ_R, the compound formation on the target surface raises until a total coverage occurs at $\Phi_R = \Phi_{R,c}$ defined as the critical flow where transition between metallic and compound mode occurs at the target (Figure 1): for $\Phi_R < \Phi_{R,c}$ the target works in the so-called "metallic mode" while for $\Phi_R > \Phi_{R,c}$, it works in the so-called "poisoned mode". This transition exhibits, most of the time, a hysteresis that can be avoided by increasing the pumping speed or reducing the target surface area.[27]

Most of the time, for $\Phi_R = \Phi_{R,c}$, R_D decreases due to numerous phenomena among which the main ones are: (i) the lower sputter yield of the compound when compared to the metal one and (ii) in most instances, the increase of the secondary electron emission coefficient, γ,

Metallic mode   **Poisoned mode**
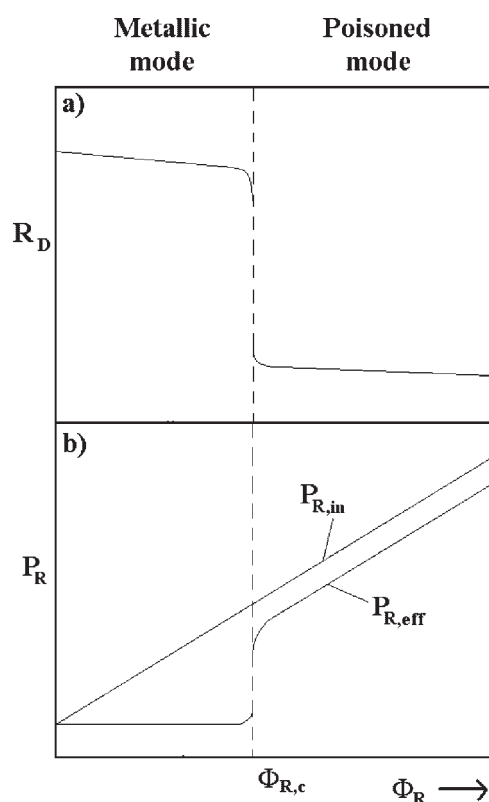
Figure 1. Typical behavior of the deposition rate, R_D, and partial pressure of reactive gas, p_R, versus the inflow rate of reactive gas, Φ_R, during a reactive magnetron sputtering experiment.

when the target surface is covered by the compound.[21] The latter phenomenon influences the plasma impedance (Z_{Plasma}) which is a decreasing function of γ. Therefore, as the current is kept constant, the target voltage (V_D) lowers, enhancing the sputter yield decrease (Figure 1a).[28]

Figure 1b shows schematically the behavior of the partial pressure of reactive gas, p_R, at the chamber input (plasma off, $p_{R,in}$) and the effective p_R (plasma on, $p_{R,eff}$) as a function of Φ_R. $p_{R,in}$ behaves linearly with Φ_R while $p_{R,eff}$ remains close to 0 for $\Phi_R < \Phi_{R,c}$ due to the trapping of the reactive gas by formation of compound on the target as well as by the metal deposited on the walls and the substrate (getter effect). When $\Phi_R > \Phi_{R,c}$, the target becomes poisoned, the consumption of reactive gas drops and $p_{R,eff}$ varies linearly with Φ_R. Nevertheless, $p_{R,eff}$ remains lower than $p_{R,in}$ because consumption of reactive gas by chemical reactions on the target and the growing film as well as ionization and reactive gas dissociation in the plasma are still occurring.

The synthesis of metal oxide films by RMS proceeds via two simultaneous mechanisms: (i) sputtering of material from the cathode and its condensation on the substrate and (ii) chemical reaction between condensing material and reactive gas species.[6,11] The ideal deposition conditions in terms of yield are reached when the second mechanism is promoted. In this case, the target is sputtered in metallic mode and RMS presents the highest deposition rate. Unfortunately, very often, the required X_{Films} is obtained for $\Phi_R > \Phi_{R,c}$.

Experimental Part

Metal oxide films were deposited on silicon wafers with a planar magnetron sputtering system (Figure 2) presenting a volume of $\approx 22.5 \times 10^{-2}$ m^3. Low pressure was reached by means of a turbomolecular-diaphragm pump combination allowing an effective pumping speed of 120 L·s^{-1} and an ultimate pressure of about 10^{-7} Torr. During deposition, Ar/O$_2$ mixtures were used as sputtering gas while sputtering pressure (p_{tot}) was maintained constant using a throttle valve. Independent mass flow controllers were used to control O$_2$ (Φ_{O_2}) and Ar (Φ_{Ar}) flows and to achieve the required fraction of O$_2$ in the discharge (f_{O_2}) following Equation (3):

$$f_{O_2} = \frac{\Phi_{O_2}}{\Phi_{Ar} + \Phi_{O_2}} \tag{3}$$

$$p_{O_2,in} = f_{O_2} * p_{tot} \tag{4}$$

Gaseous flows were adapted to maintain a constant total gas flow (Φ_{tot}) in the chamber. Input O$_2$ partial pressure ($p_{O2,in}$) is given by Equation (4). Table 1 summarizes, among others, the gaseous conditions used during the experiments.

Metallic disks (2 inch in diameter) of Ag, Ti and Sn (99.99% purity) were used as targets and a DC power supply (MDX 500
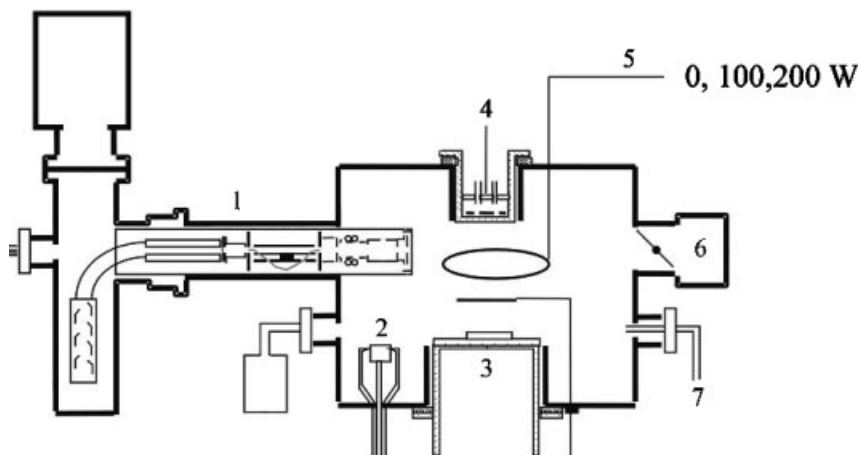
Figure 2. Experimental setup: mass spectrometer (1), quartz microbalance (2), substrate holder (3), target (4), RF coil (5), throttle valve (6), gas supply (7).

from Advanced Energy) working in the current regulation mode was powering the magnetron cathode. Neutralization of cathodic arcs during the deposition process was performed using the Sparc-Le 20 system from Advanced Energy. Table 1 reports the current (I_D) and the current density applied to the cathode (I_d) for each experiment.

The induction coil was a ring made of a copper tube of 6 mm in diameter. One tip was grounded and the other connected by a coaxial line to the RF generator. The ring was located 5 cm in front of the cathode and was powered by a 13.56 MHz generator (Huttingër PFG 300rf) coupled with a matching box (Huttingër tuning network PFM 400A). The power delivered to the coil (P_{RF}) varied from 0 to 200 W.

Ionic and neutral species concentrations in the plasma were measured using a differentially pumped quadrupole Balzers PPM 421 mass spectrometer with an integrated ion energy analyzer.[29] Neutral species were measured using residual gas analysis mode (RGA) while glow discharge mass spectrometry (GDMS) was performed to assess the ion energy distribution and the relative density of positive ions present in the plasma. The measured signals were corrected for the mass (m) of the measured species ($\sim m^{-1/2}$).

R_D was measured by following the deposited mass on a quartz microbalance located close to the substrate (Figure 2) and the film composition, X_{Films}, was determined by XPS without contamination since the samples were transferred under high vacuum into the XPS analysis chamber.

XPS was performed on a VG - ESCALAB 220iXL spectrometer. The pressure in the analysis chamber was typically 8×10^{-11} Torr. XPS measurements were obtained using monochromatic Al-K_α radiation at 1 486.6 eV. The energy resolution of the spectrometer was about 0.5 eV. The photoelectrons were collected from a $250 \times 1\,000\ \mu m^2$ sample area at a take-off angle, $\Phi = 0°$ from the normal to the surface (normal detection). For each measurement, survey spectra were recorded with a 50 eV pass energy, as well as high resolution spectra (20 eV pass energy) in the regions of interest (O 1s, Ag 3d, Sn 3d and Ti 2p). Atomic compositions were derived from peak areas using the photo-ionization cross-section

calculated by Scofield,[30] corrected (i) for the dependence of the escape depth λ on the electron kinetic energy (assumed to have the form $\lambda = KE^{0.6}$) and (ii) for the analyzer transmission function of the spectrometer analyzer.

Results and Discussion

Target Surface Chemistry

Target surface composition, X_{Target}, is evaluated from target voltage (V_D) and deposition rate (R_D) measurements.[11,31–33] V_D variations are correlated to plasma impedance, Z_{Plasma}, which depends mainly on plasma ionization. As X_{Target} influences the secondary electron emission coefficient, γ, and as constant discharge current mode is used, decreasing γ leads to an increase of V_D. Since variations of V_D influence R_D by modifying the sputter yield, it is accepted that, as V_D decreases when target becomes poisoned, target poisoning is correlated to a dramatic decrease of R_D.

The change of V_D with $pO_{2,in}$ is interpreted by using Depla's model for target surface chemistry modification in reactive plasmas.[14,31,34,35] This model,[36–38] experimentally verified,[39] considers two mechanisms during target poisoning: (i) chemisorption of reactive species on the target surface and (ii) implantation of reactive ions in the near surface of the target. The authors suggest that target poisoning occurs in the outermost target surface (a few nm) mainly by chemical reactions between reactive ions implanted and metallic atoms composing the target. At a critical implantation dose and if the metal reactivity, ξ_M, is high enough, compound formation occurs.[36] Moreover they have shown, for Al-Ar/O$_2$ discharges, that reactive gas chemisorption can play a significant role, especially at low input partial pressure of O$_2$, $p_{O2,in}$. Indeed, before oxide formation, a chemisorbed layer of reactive gas is formed and the onset of oxidation begins only after the surface is completely covered by a chemisorbed reactive gas monolayer.[40] In this case (Al-Ar/O$_2$), the exposure to reactive gas needed for covering the Al target has been determined at about 100 Langmuir.

The target poisoning mechanism during RMS is obviously correlated to the reactivity of the metal to oxygen, ξ_M. Indeed, depending on ξ_M, two extreme situations are observed: (i) ξ_M is high: chemisorption is strong; reactive implantation leads to compound formation,[40] and (ii) ξ_M is low: no chemisorption occurs; reactive implantation occurs, but without compound formation. In this case, molecular gas desorption can be observed.[34]

Synthesis of Metal Oxide Thin Films by Reactive Magnetron Sputtering in Ar/O₂ Mixtures: . . .

Plasma Processes
and Polymers
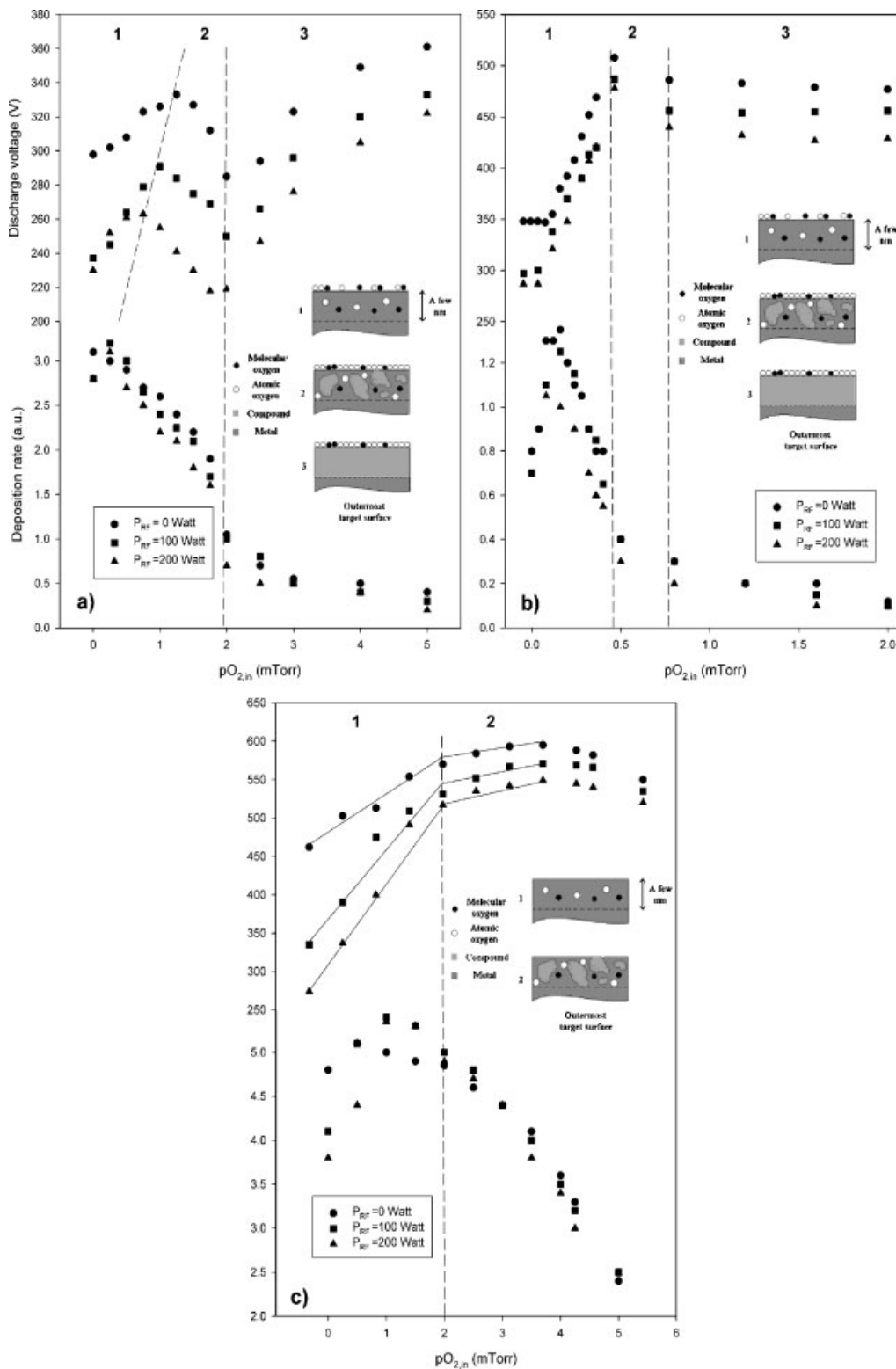
Figure 3. Discharge voltage and deposition rate behavior versus the input partial pressure of O₂, $p_{O2,in}$, for conventional and amplified RMS in the case of Sn-Ar/O₂ (a), Ti-Ar/O₂ (b) and Ag-Ar/O₂ (c) systems.

Figure 3 reports the evolutions of V_D and R_D as a function of $p_{O2,in}$ for Sn-Ar/O_2 (Figure 3a), Ti-Ar/O_2 (Figure 3b), and Ag-Ar/O_2 (Figure 3c) in conventional and iRMS discharges. To facilitate the interpretation, the curves are divided in 3 regions (1, 2 and 3).

Sn-Ar/O_2

Figure 3a shows that, increasing P_{RF}, V_D shifts toward lower values over all the range of $pO_{2,in}$. This phenomenon is attributed to the increase of the plasma ionization level leading to a decrease of Z_{Plasma}. Concerning the change of V_D with $p_{O2,in}$: for each value of P_{RF}, V_D increases sharply until a maximum is reached (region 1), then decreases until a minimum (region 2) and finally increases again (region 3).

The initial increase is attributed to chemisorption of reactive species (O, O_2) on the target surface since it is known that oxygen chemisorption on metal surfaces generally decreases γ.[41] Simultaneously, reactive ions begin to be implanted in the outermost target surface but the dose is still too low so that the compound cannot be formed. The maximum is reached when the chemisorbed layer is achieved on the target surface. It can be assumed that, regarding its higher reactivity,[12,13] highlighted by its higher reaction coefficients on Sn and SnO,[32] O is probably more rapidly chemisorbed than O_2. Therefore, the shift of the V_D maximum towards lower $p_{O2,in}$ as P_{RF} increases is attributed to the increase of the atomic oxygen density (n_O) with P_{RF} (see later), leading to a full coverage of the target surface by reactive species at lower $p_{O2,in}$

Since V_D and reactive ions densities (O^+ and O_2^+) increase with $p_{O2,in}$,[39] reactive ions implantation becomes more and more significant and compound formation occurs. Therefore, the decrease of V_D in region 2 is attributed to target poisoning. The minimum of V_D between regions 2 and 3 corresponds to the complete target poisoning and does not depend on P_{RF}. As it is pointed out in the introduction, reactive species ionization is less influenced by the RF coil plasma than the metallic ones because of their higher ionization thresholds. Thus, it is assumed that the independence of target poisoning on P_{RF} is a result of the weak effect of the secondary plasma on the reactive ion density.

When target is completely poisoned (region 3), V_D depends mainly on variations in the gas phase composition: the plasma contains more and more O_2 which decreases n_e by electronic capture reactions to form O_2^-.[43] Moreover, it has been shown that n_e and T_e decrease when O_2 concentration increases[22] leading to a decrease in the plasma ionization level and in turn to an increase of V_D in order to maintain the discharge current constant.

R_D behaves like V_D, namely it shifts toward lower values when P_{RF} increases. This evolution is related to V_D: since V_D decreases, the sputtering yield lowers and consequently R_D decreases too. Concerning its dependence on $p_{O2,in}$, R_D presents, for each P_{RF}, a maximum which is attributable to the getter effect of the condensed metal on the micro-balance and to the increase of V_D in this region. Since the target becomes poisoned, R_D decreases substantially (region 2) until a stable value is reached. When using iRMS, the behaviour of R_D is compatible with the target surface composition, X_{Target}, evolution deduced from V_D behaviour. Indeed, similarly to V_D, the sharp decrease of R_D induced by target poisoning shows no dependence on P_{RF} (Figure 3a).

Ti-Ar/O_2

On the whole, interpretations of both V_D and R_D evolutions as a function of $p_{O2,in}$ (Figure 3b) are similar to the ones proposed for Sn-Ar/O_2. Nevertheless, the efficiency of the oxidation mechanisms at the target is quite higher since $\xi_{Ti} > \xi_{Sn}$. For example, covering of the target surface by reactive species (maximum of V_D) is reached for $p_{O2,in} \approx 0.4$ mTorr and target poisoning (region 3) for $p_{O2,in} \approx 0.8$ mTorr. For Sn-Ar/O_2, these phenomena occur for $p_{O2,in} \approx 1$ mTorr and $p_{O2,in} \approx 2$ mTorr, respectively (Figure 3a).

Another striking difference is the independence on P_{RF} of the maximum of V_D attributed to the covering of the target surface by chemisorbed reactive species. Again, this could be explained by the high value of ξ_{Ti}: for Ti, chemisorptions of both O and O_2 are efficient. This is supported by previous reports where reaction coefficients of O and O_2 on Ti and TiO_2 surface have been determined to be similar.[43] Consequently, an increase of n_O does not raise the chemisorption rate like for Sn-Ar/O_2.

The change of R_D is quite similar to that of Sn-Ar/O_2 with a maximum at low $p_{O2,in}$ (getter effect, V_D increase). The transition between the metallic and the compound sputter regimes shows no dependence on P_{RF} (Figure 3b).

Ag-Ar/O_2

For Ag-Ar/O_2 (Figure 3c), similarly to Sn-Ar/O_2 and Ti-Ar/O_2, increasing $p_{O2,in}$ leads to an initial increase of V_D (region 1) but no decrease is observed at higher $p_{O2,in}$. The maximum of V_D (between zone 1 and 2) is attributed, in this case, to reactive species implantation. Similar behaviour has been observed by Depla et al. when studying Ag-Ar/N_2 system.[34] This assumption is supported by the independence of the position of the maximum on P_{RF} proving the reactive ion-conducted process. Moreover, since ξ_{Ag} is quite lower than ξ_{Ti} and ξ_{Sn}, chemisorptions of reactive species should be very limited. Again, this is consistent with previous works reporting very low reaction coefficients for O and O_2 on Ag and Ag oxides surfaces.[44]

Despite the fact that we do not observe any decrease of V_D, we assume that, for a certain $p_{O2,in}$ (corresponding to the value at which the slope changes on the V_D curves),

Synthesis of Metal Oxide Thin Films by Reactive Magnetron Sputtering in Ar/O₂ Mixtures: . . .

Plasma Processes
and Polymers

compound formation occurs on the Ag target surface. This is supported by the decrease of R_D for $p_{O2,in} > 2$ mTorr (region 2). Therefore, it is assumed that, in the case of Ag, the secondary electron emission coefficient, γ, is lower for the compound than for the metal. Ag compound formation on the target is confirmed by GDMS measurements as we show later in this paper.

Chemistry of the Plasma

Reactive Gas Composition

We estimated $p_{O2,eff}$ using RGA measurements. For each Ar/O₂ mixture, two measurements were performed. The first one consists of measuring RGA signal at the mass/charge ratio $(m/z) = 32$ (corresponding to O₂) with no plasma. This allows to calibrate the mass spectrometer in term of p_{O2} since without plasma, no O₂ is consumed. The second measurement is conducted in the same gaseous conditions with DC or DC+RF plasmas switched on. $p_{O2,eff}$ is calculated from the signal at $m/z = 32$ using the calibration coefficient determined from the first experiment.

Figure 4 reports, for example, the results obtained for Ti-Ar/O₂: $p_{O2,eff}$ remains close to 0 until the critical point corresponding to target poisoning. Before this point, all O₂ introduced in the chamber is consumed. One can remark that the critical value appears for a value of $p_{O2,in}$ (0.4 mTorr) very close to the one determined from V_D and R_D measurements (Figure 3b). This behaviour is qualitatively predicted by all the theoretical models[11–13,22] as was discussed in the introduction. A similar behaviour is observed for Sn-Ar/O₂ with, obviously, differences for both the value of the critical point and the consumption level since ξ_{Ti} and ξ_{Sn} are different. For Ag-Ar/O₂, at the contrary, nearly linear evolution of $p_{O2,eff}$ with $p_{O2,in}$ is observed.
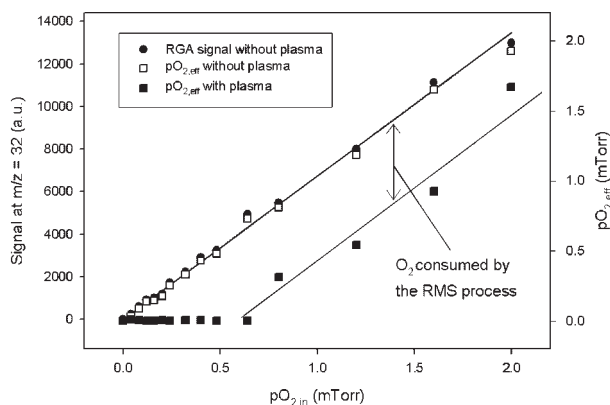
Figure 4. Example of determination of the effective partial pressure of O₂, $p_{O2,eff}$ and the input O₂ consumed by the process, $O_{2,cons}$, from RGA measurements (conventional RMS of Ti-Ar/O₂).
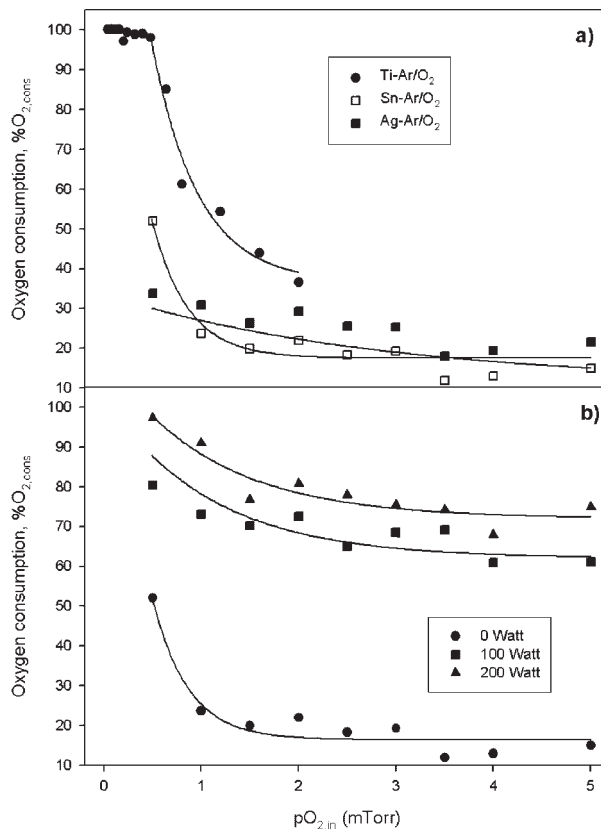
Figure 5. Evolution of the input O₂ consumed by the process, $O_{2,cons}$, versus the input partial pressure of O₂, $p_{O2,in}$, for the different studied systems in conventional RMS (a) and for iRMS in the case of Sn-Ar/O₂ (b).

To highlight these results, we defined the percentage of O₂ consumed by the process ($O_{2,cons}$) from Equation (5). Figure 5 presents the behaviour of $O_{2,cons}$ as a function of $p_{O2,in}$ for the different systems in a conventional RMS plasma (Figure 5a) and for different P_{RF} in the case of Sn-Ar/O₂ discharge (Figure 5b):

$$O_{2,cons} = \frac{p_{O2,in} - p_{O2,eff}}{p_{O2,in}} \qquad (5)$$

As expected, $O_{2,cons}$ behaves differently depending on ξ_M. For Ti-Ar/O₂, O₂ is practically completely consumed before the critical point. For higher $p_{O2,in}$, $O_{2,cons}$ decreases sharply until $\approx 40\%$ which corresponds to an equilibrium value when X_{Target} stabilizes. For Sn-Ar/O₂ the consumption is lower but, conceptually, the evolution of $O_{2,cons}$ is the same as for Ti-Ar/O₂ with a stabilization for $O_{2,cons} \approx 20\%$. Finally, for Ag-Ar/O₂, the sharp decrease at low $p_{O2,in}$ is not observed and $O_{2,cons}$ behaves nearly linearly with $p_{O2,in}$.

On Figure 5b is reported the evolution of $O_{2,cons}$ with different P_{RF} for Sn-Ar/O₂ system. The shape of the curve is

not influenced by P_{RF} but the level of consumption is clearly increased. We attribute this increase to the higher O_2 dissociation using iRMS. Indeed, in a RMS discharge (conventional or amplified), O_2 consumption occurs by three main mechanisms: (i) chemical reaction on target and/or the growing film, (ii) dissociation and (iii) ionization.[42] For metals presenting the highest ξ_M, the first mechanism (i) is the most important and depends on X_{Target} and thus on $p_{O2,in}$ while both dissociation and ionization processes depend on T_e and n_e.[12,13] Considering these mechanisms, evolution of $O_{2,cons}$ as a function of $p_{O2,in}$ can be explained.

For Ag-Ar/O_2, the linear evolution of $O_{2,cons}$ means that consumption of O_2 by chemical reaction on both target and growing film remains low, even at low $p_{O2,in}$. Consequently, we assume that the main consumption processes are, in this case, ionization and dissociation of O_2. The decrease of $O_{2,cons}$ could be associated to the decrease of both n_e and T_e when $p_{O2,in}$ increases as it has been proposed by Trennepohl et al.[22]

On the contrary, for Sn-Ar/O_2 and Ti-Ar/O_2, and especially at very low $p_{O2,in}$, O_2 is mainly consumed on the target and the growing film. Indeed, using iRMS, T_e and mainly n_e increase leading to higher ionization and dissociation of O_2.[15–17] On the contrary, the sputtering yield is not influenced by the higher plasma ionization in a measurable way.[42] Consequently, the amount of condensing material which can be oxidized by the reactive species present in the plasma does not depend on P_{RF}. Considering the binding energy (5.08 eV) and the ionization threshold of O_2 (12.15 eV), it can be assumed that using iRMS, the dissociation process is, above all, affected.

Metallic Vapor Composition

In order to optimize the GDMS signal, mass spectrometry measurements were performed for an energy corresponding to the maximum of the ion energy distribution. This energy is similar whichever ionized particles are considered.[45] For example, Figure 6 shows a mass spectrum measured for Ag-Ar/O_2 (conventional RMS) with $p_{O2,in} = 3$ mTorr. Species related to the sputtering gas mixture (O^+, Ar^+, O_2^+, Ar_2^+, ...) and coming from the target sputtering process (Ag^+, AgO^+, $AgAr^+$, Ag_2O^+, ...) are observed. This spectrum proofs that, despite the low value of ξ_{Ag} and the weak consumption of O_2 measured in this case (Figure 5), a compound is really formed on the Ag target surface inducing a decrease of R_D (Figure 3c).

From such GDMS spectra, the molar fraction of metal oxide species (x_{MO_n}) is calculated using Equation (6):[46]

$$x_{MO_n} = \frac{I_{MO_n^+}}{\sum_{n=0}^{i} I_{MO_n^+}} \quad \text{with} \quad \sum_{n=0}^{i} x_{MO_n} = 1 \quad (6)$$
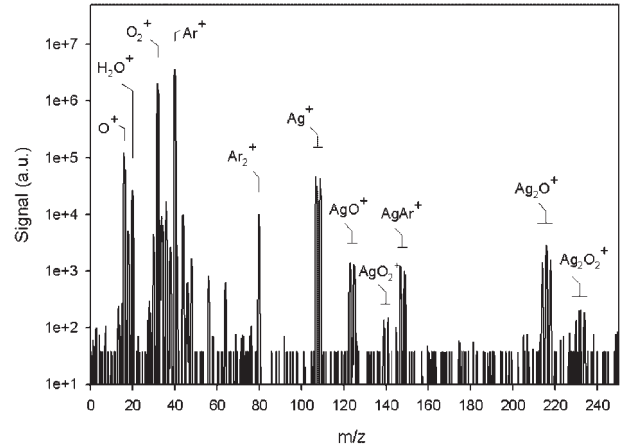
Figure 6. Example of mass spectrum measured in Ag-Ar/O_2 in conventional reactive magnetron sputtering, the input partial pressure of O_2, $p_{O2,in}$, is 3 mTorr.

in which n is the number of oxygen atom present in the ionic metallic species MO_n^+ and $I_{MO_n^+}$ the GDMS signal corresponding to this species. On the other hand, the plasma composition, X_{Plasma}, is defined as the ratio between oxygen and metal atom concentrations in the metallic species present in the plasma [(Equation (7)].

$$X_{Plasma} = \frac{[O]}{[M]} \quad (7)$$

Considering Equation (4), this equation can be rewritten for Sn-Ar/O_2 as Equation (8), Ti-Ar/O_2 as Equation (9) and Ag-Ar/O_2 as Equation (10):

$$X_{Plasma}(Sn) = \frac{x_{SnO} + 2x_{SnO_2}}{x_{Sn} + x_{SnO} + x_{SnO_2}} = x_{SnO} + 2x_{SnO_2} \quad (8)$$
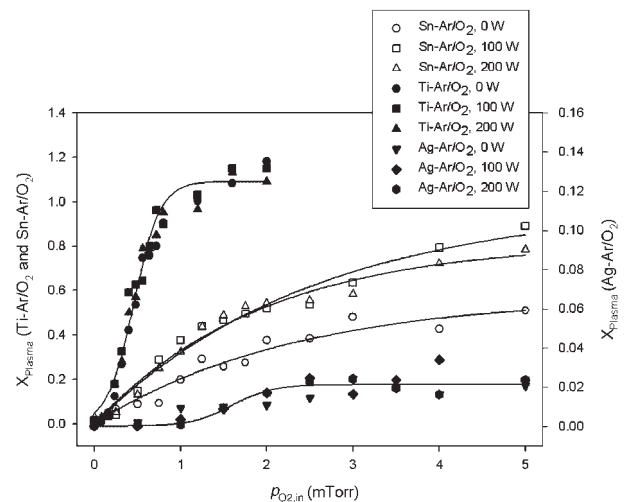
Figure 7. Plasma composition, X_{Plasma}, versus the input partial pressure of O_2, $p_{O2,in}$, for conventional and iRMS processes.

Synthesis of Metal Oxide Thin Films by Reactive Magnetron Sputtering in Ar/O₂ Mixtures: . . .

Plasma Processes
and Polymers
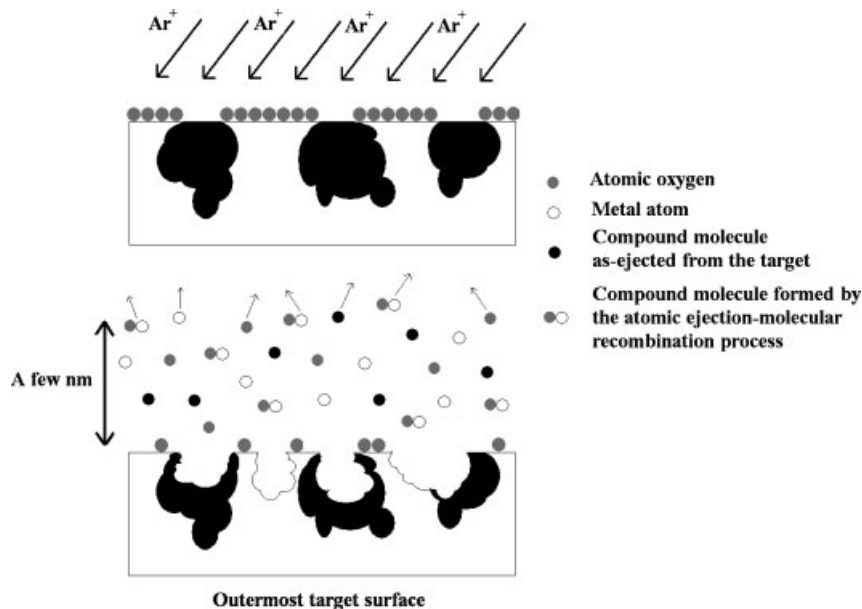
Figure 8. Atomic ejection/molecular recombination process.

$$X_{Plasma}(Ti) = \frac{x_{TiO} + 2x_{TiO_2}}{x_{Ti} + x_{TiO} + x_{TiO_2}} = x_{TiO} + 2x_{TiO_2} \qquad (9)$$

$$X_{Plasma}(Ag) = \frac{x_{AgO} + x_{Ag_2O}}{x_{Ag} + x_{AgO} + 2x_{Ag_2O}} \qquad (10)$$

Since in the range of p_{Tot} in which we worked (5–8 mTorr) the probability of chemical reaction inside the plasma is very low,[21,47] it is assumed that X_{Plasma} is correlated to the target surface composition, X_{Target}.[48]

Figure 7 reports the evolution of X_{Plasma} in both conventional and iRMS discharges. The sputter gas
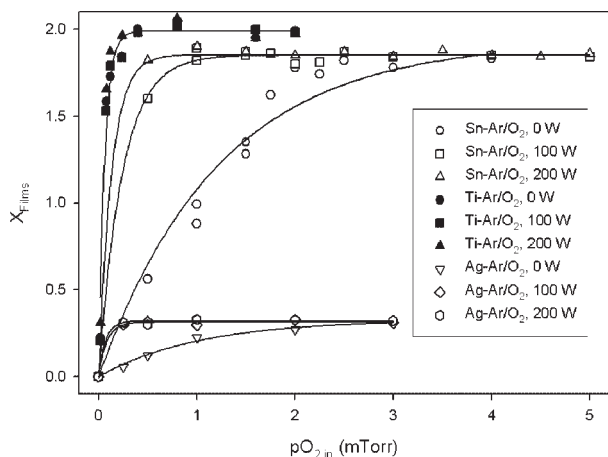
Figure 9. Film composition, X_{Films}, versus the input partial pressure of O₂, $p_{O2,in}$, for conventional and iRMS processes.

mixture composition influences dramatically X_{Plasma}. In every cases, X_{Plasma} increases with $pO_{2,in}$ until a plateau is reached when X_{Target} stabilizes. This plateau appears for $X_{Plasma} = 0.02$ for Ag-Ar/O₂, $X_{Plasma} = 1.2$ for Ti-Ar/O₂ and $X_{Plasma} = 0.4$ to 0.8 depending on P_{RF} for Sn-Ar/O₂.

R_D measurements show that, for all the systems, target poisoning is not influenced by the higher plasma reactivity (Figure 3). Considering the correlation between X_{Plasma} and X_{Target}, X_{Plasma} should also be independent of P_{RF}. This has been observed for Ag-Ar/O₂ and Ti-Ar/O₂ but surprisingly, for Sn-Ar/O₂, we observed an increase of X_{Plasma} with P_{RF}, especially between $P_{RF} = 0$ and 100 W. This peculiar behaviour is attributed to the dependence, on plasma reactivity, of the atomic oxygen adsorption own the Sn target surface.

The latter phenomenon is explained by considering another mechanism for the production of compound species observed in the plasma than the conventional ejection of compound molecules from the poisoned cathode. This mechanism, called "atomic ejection-molecular recombination mechanism" schematically described on Figure 8, was originally demonstrated using secondary ion mass spectrometry experiments by Honda et al. and Garrison et al.[49,50] In a few words, after ionic impact on the target surface, the impinging ion transfers a fraction of its kinetic energy to particles composing the target but also to the ones chemisorbed on the surface. During a short period of time after the impact ($\approx$1 ps), a high density of particles is present in a confined space near the cathode surface (a few nm). These particles (i and j) can react together to form molecules if Equation (11) is obeyed. $(E_{ij})_K$ is the relative kinetic energy and $(E_{ij})_P$, the interaction potential energy.

$$\sum_{ij} ((E_{ij})_K + (E_{ij})_P) < 0 \qquad (11)$$

Considering this mechanism and the influence of P_{RF} on the chemisorptions of reactive species (mostly O) on Sn target surface (Figure 3a), it can be explained that, despite the independence of target poisoning on P_{RF}, X_{Plasma} depends on it. This behaviour is not observed for Ti-Ar/O₂ and Ag-Ar/O₂ because in these cases, even if the adsorption of reactive species on the target surface also occurs (at least for Ti), it shows no dependence on P_{RF} while for these systems, no shift of V_D maximum is observed (Figure 3b and 3c).

Table 2. Comparison between experimental and published data for binding energy [eV] measured by XPS.

Metal	Peak	Experimental data	Data from the literature			Ref.
Sn	$3d_{5/2}$	486.3	Sn^0	Sn^{2+}	Sn^{4+}	
			484.9	485.4–486.9	486.2–486.6	[51]
Ti	$2p_{3/2}$	459.3	Ti^0	Ti^{2+} $\quad$ Ti^{3+}	Ti^{4+}	
			454.1–453.9	455.3 $\quad$ 457.2	458.7–459.2	[52]
Ag	$3d_{5/2}$	367.9	Ag^0	Ag^+	Ag^{2+}	
			368.2	367.8–368.4	367.4–368	[53]
	Auger (M_5NN)	350.4 and 351.5	351.6	350.6	350.6	[53]

Chemistry of the Deposited Film

The film composition, X_{Films}, is investigated by XPS and calculated from Equation (12) in which O_2 at.% and M at.% are the atomic percentage of O_2 and M in the deposited films, respectively.

$$X_{\text{Films}} = \frac{O_2 \quad \text{at.\%}}{M \quad \text{at.\%}} \tag{12}$$

Figure 9 reports X_{Films} as a function of $p_{\text{O2,in}}$, for each system in conventional and iRMS discharges. In every case, increasing $p_{\text{O2,in}}$, X_{Films} increases sharply up to a plateau corresponding to the maximum stoichiometry of the film (X_{FC}). $X_{\text{FC}} = 2$, 1.8 and 0.34 for Ti-Ar/O_2, Sn-Ar/O_2 and Ag-Ar/O_2 respectively. For Sn-Ar/O_2, X_{FC} is limited by the gaseous conditions used in this work. As we showed in a previous work, the "full stoichiometry" $X_{\text{FC}} = 2$ can only be reached at higher $p_{\text{O2,in}}$.[32] The presence of several oxidation states in the films is confirmed by the electron

binding energy (BE) of the metal peak. These measurements are compared to literature data in Table 2.

For $X_{\text{FC}} = 2$, Ti $2p_{3/2}$ peak (459.3 eV) proves that only Ti^{4+} species are present, confirming the complete oxidation of the film. For tin oxide films, Sn $3d_{5/2}$ peak at 488.3 eV is observed. Due to the small difference of BE between Sn^{2+} and Sn^{4+}, it is not possible to determine precisely the oxidation level of tin. Nevertheless, all tin species are oxidized since we did not observe any signal at BE = 484.9 eV corresponding to metallic tin (Sn^0). This is coherent with the quantification results ($X_{\text{FC}} = 1.8$). Therefore, we assume that a mixture of Sn^{2+} and Sn^{4+} species composes the tin oxide films. Finally, for silver oxide films, we can not confirm Ag oxidation by XPS measurements because the BE of Ag^0, Ag^+ and Ag^{2+} are too close to each other (Table 2). Nevertheless, in the Auger region, two components in the M_5NN Auger peak are observed at 351.5 eV and 350.5 eV corresponding to metallic and oxidized Ag species, respectively.[53] This confirms the presence of a mixture of Ag^+ and/or Ag^{2+} and Ag^0 in the deposited films.

Table 3. Parameters determined from the fit with Equation (13) of curves presented on Figure 9. P_{RF} is the RF power applied to the coil, X_{FC} is the full stoichiometry of the film and k_{ox} is a reactive species-growing film reaction parameter.

Metal	P_{RF} W	X_{FC}	k_{ox} mTorr^{-1}	$R^{2a)}$
Sn	0	1.93	1.5	0.981
	100	1.85	7.8	0.998
	200	1.86	14.3	0.999
Ti	0	1.99	32.4	0.982
	100	1.99	32.2	0.983
	200	2	32	0.986
Ag	0	0.33	0.3	0.995
	100	0.31	4.0	0.997
	200	0.32	4.8	0.997

a)Correlation coefficient.
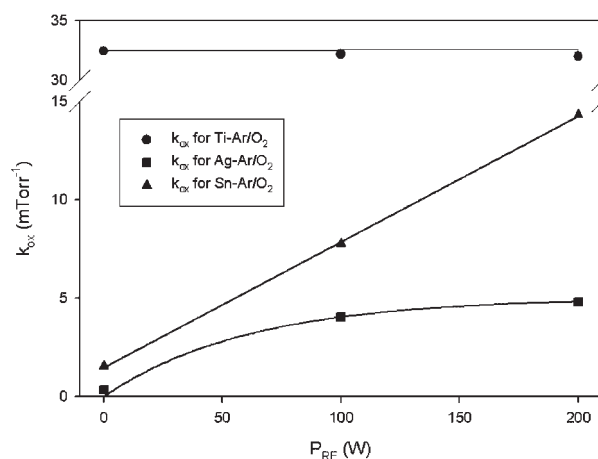
Figure 10. Reactive sputtering-growing film reaction parameter, k_{ox}, versus the RF power applied to the coil, P_{RF}, for conventional and iRMS processes.

Synthesis of Metal Oxide Thin Films by Reactive Magnetron Sputtering in Ar/O₂ Mixtures: . . .

Plasma Processes
and Polymers

For all conditions and systems, X_{Films} as a function of $p_{O2,\text{in}}$ is fitted with an exponential function [Equation (13)]:

$$X_{\text{Films}} = X_{\text{FC}}\left(1 - e^{\frac{k_{\text{ox}}}{X_{\text{FC}}}p_{O2,\text{in}}}\right), \qquad (13)$$

where the parameter k_{ox} is related to the adsorption reaction of oxygen (O, O₂) by the growing film. Actually, k_{ox} defines the shape of X_{Films} curves at very low $p_{O2,\text{in}}$, before poisoning, when target is still metallic and adsorption reaction on growing films is predominant. k_{ox} depends on the metal reactivity to oxygen, ξ_M, and on the densities of reactive species present in the plasma. Nevertheless, since atomic oxygen has substantially higher reaction coefficient than molecular oxygen,[12,13,32,43,44] k_{ox} is mainly dependent on the density of atomic oxygen. k_{ox} determined from X_{Films} curves fitting are reported in Table 3. Comparison of k_{ox} for the different systems in conventional discharges shows that, as it could be expected, k_{ox} increases with ξ_M.

Evolution of k_{ox} as a function of P_{RF} for each system is presented in Figure 10. k_{ox} behaves differently depending on the metal considered. For Sn-Ar/O₂, k_{ox} increases linearly with P_{RF}. This demonstrates the improvement of the oxidation mechanism of the growing film by increasing n_O in iRMS discharges. Indeed, since n_O increases for a given $p_{O2,\text{in}}$, adsorption of atomic oxygen on the growing film is improved while target poisoning, occurring by reactive ions implantation, remains constant as it was shown from V_D and R_D measurements (Figure 3a).

For Ti-Ar/O₂, at the contrary, k_{ox} does not depend on P_{RF}. In this case, the reactions of the growing film with both atomic and molecular oxygen are very efficient as we showed previously.[43] Thus, increase of n_O using iRMS plasma does not affect the reactive gas adsorption reaction on the growing film and therefore k_{ox} does not change with P_{RF}.

Finally for silver, k_{ox} increases until a plateau which appears for $P_{\text{RF}} \approx 120$ W. In this case the reactive gas adsorption reaction on the growing films is improved by increasing n_O using iRMS plasma. Indeed, contrary to titanium, silver films oxidize almost only by atomic oxygen species, since the reaction coefficient of O₂ on silver is close to 0.[44] Nevertheless, in this case, for a given n_O (corresponding to $P_{\text{RF}} \approx 120$ W), the very low ξ_{Ag} becomes the limiting factor of the process since further increase of n_O does not improve the oxidation reaction at the substrate. It could be assumed that a similar plateau should appear at higher P_{RF} in the case of Sn-Ar/O₂. We were not able to verify this assumption since 200 W was the maximum RF power which can be applied to the RF coil.
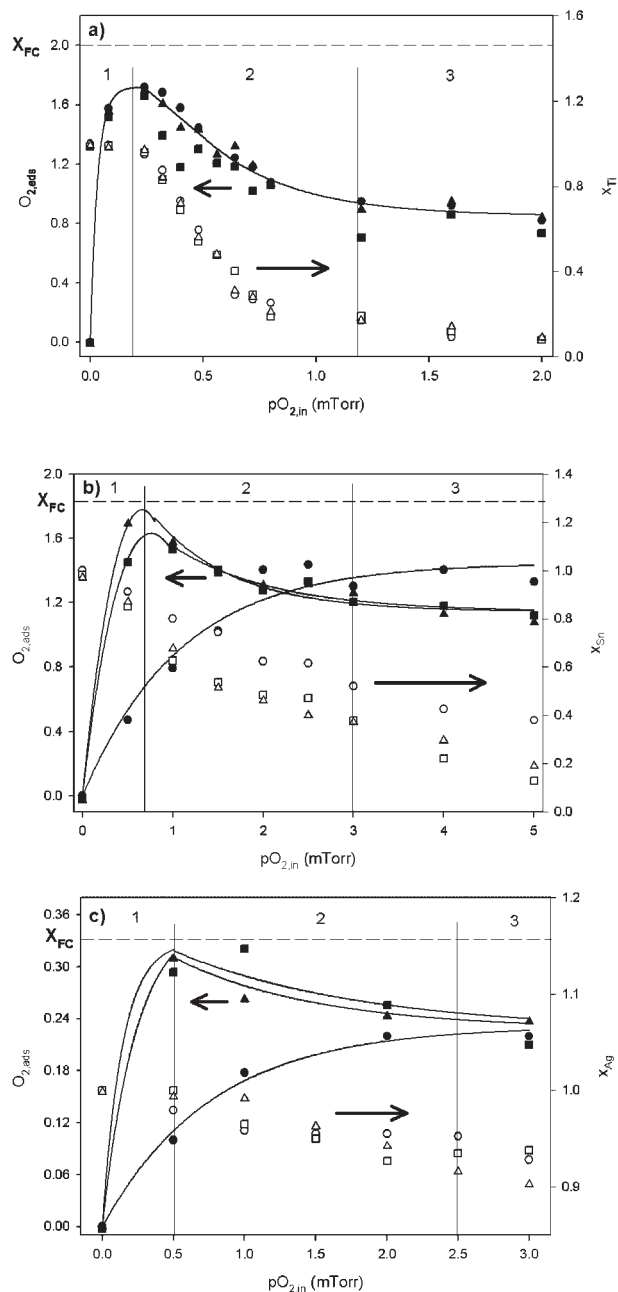
Figure 11. Oxygen incorporated by adsorption reaction on the growing film, O₂,ads, versus the input partial pressure of O₂, $p_{O2,\text{in}}$, for conventional and iRMS processes for Ti-Ar/O₂ (a), Sn-Ar/O₂ (b) and Ag-Ar/O₂ (c). Filled symbols are related to O₂,ads and unfilled to the molar fraction of metal in the plasma, x_M. Circles, squares and triangles correspond to measurements at RF power applied to the coil, P_{RF}, of 0 W, 100 W and 200 W, respectively.

Mechanism of Synthesis

Combining the results obtained from the studies of both the plasma and the film chemistries, we quantified the relative importance of the two simultaneous mechanisms

involved in the film synthesis. The film composition (X_Films) is reached by condensation of sputtered particles (X_Plasma) and by oxidation reactions between the condensing material (M, MO) and the reactive species present in the plasma (O, O$_2$). Therefore, synthesis of oxide compounds by RMS can be described by Equation (14):

$$X_\text{Films} = X_\text{Plasma} + \alpha_1^0[M]p_O + \alpha_1^1[MO]p_O$$
$$+ \alpha_2^0[M]p_{O_2} + \alpha_2^1[MO]p_{O_2,} \tag{14}$$

in which α_i^j are the reaction coefficients of the different species. $i = 1$ and 2 for atomic and molecular oxygen, respectively and $j = 0$ and 1 for M and MO species, respectively. p_O and p_{O_2} are the partial pressures of O and O$_2$ and [M] and [MO] are the concentration of M and MO on the substrate.

In order to determine the relative importance of one mechanism against the other, the proportion of oxygen incorporated in the oxide films by reaction with the condensing material is determined (O$_{2,\text{ads}}$) according to Equation (15):

$$O_{2,\text{ads}} = X_\text{Films} - X_\text{Plasma}$$
$$= \alpha_1^0[M]p_O + \alpha_1^1[MO]p_O + \alpha_2^0[M]p_{O_2}$$
$$+ \alpha_2^1[MO]p_{O_2} \tag{15}$$

Figure 11 reports O$_{2,\text{ads}}$ as a function of $p_{O2,\text{in}}$ for each system in conventional and iRMS discharges. On the same graph, the molar fraction of metal present in the plasma, x_M, is plotted: it is assumed to be proportional to [M].[54] To facilitate the interpretation, the curves are divided into 3 regions (1, 2, 3).
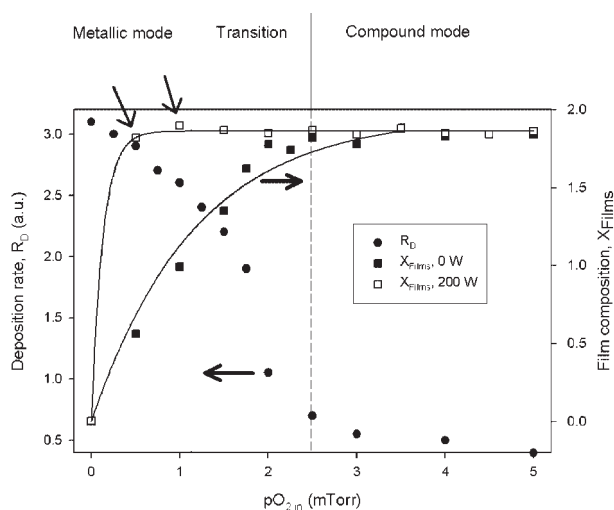
Figure 12. Demonstration of the technological advantage of using the discharge amplification in reactive magnetron sputtering in the case of Sn-Ar/O$_2$ discharges.

Table 4. Effect of plasma amplification on the deposition rate of full oxidized films. P_RF is the RF power applied to the coil, $p_{O2,\text{in}}$ is the input partial pressure of O$_2$ for which X_FC is reached, X_FC is the full stoichiometry of the film and R_D is the deposition rate.

Metal	P_RF	$pO_{2,\text{in}}$	R_D
	W	mTorr	u.a
Sn	0	3.5	0.52
	100	1.8	1.70
	200	0.5	2.95
Ti	0	0.5	0.42
	100	0.5	0.37
	200	0.5	0.36
Ag	0	3	4.35
	100	2	5.00
	200	1	5.35

The evolution of O$_{2,\text{ads}}$ with $p_{O2,\text{in}}$ depends on the studied system and on P_RF. The simplest case is the one of Ti-Ar/O$_2$ (Figure 11a) for which the secondary plasma does not affect adsorption reaction. At very low $pO_{2,\text{in}}$ (region 1), O$_{2,\text{ads}}$ increases sharply with $p_{O2,\text{in}}$ since in this region, condensing species are mainly metallic as shown by x_Ti value. A maximum is reached for $p_{O2,\text{in}} = 2$ mTorr just before target poisoning occurs. Then, O$_{2,\text{ads}}$ decreases (region 2) to finally stabilizes (region 3).

The maximum corresponds to the "ideal" gaseous conditions for which reaction between the condensing compound and reactive species is promoted against target poisoning. Unfortunately, this maximum value remains lower than X_FC meaning that, for Ti-Ar/O$_2$, some supply of oxidized sputtered species from poisoned cathode is inevitable. Actually, the high value of ξ_Ti leads to compound formation on target surface even at very low $p_{O2,\text{in}}$. The subsequent decrease of O$_{2,\text{ads}}$ occurs by supply of oxidized species from target compound sputtering to the growing film.

For Sn-Ar/O$_2$ (Figure 11b) and Ag-Ar/O$_2$ (Figure 11c), the evolutions of O$_{2,\text{ads}}$ with $p_{O2,\text{in}}$ are qualitatively similar. For conventional discharges, the evolution of O$_{2,\text{ads}}$ does not present the maximum observed for Ti-Ar/O$_2$. This means that before target poisoning, reactions between reactive species and condensing metal atoms are not efficient (region 1). The low reaction coefficients of O$_2$ with both Sn and Ag explain this behaviour.[32,44] Indeed, in these cases, as n_O remains low (conventional RMS), oxidation of the growing film is weak.

Using iRMS, for both systems, the evolution of O$_{2,\text{ads}}$ is similar to the one of Ti-Ar/O$_2$ with appearance of a maximum between regions 1 and 2. Since, on the one hand, for both systems, x_M does not depend on P_RF in region 1 and,

Synthesis of Metal Oxide Thin Films by Reactive Magnetron Sputtering in Ar/O$_2$ Mixtures: . . .

Plasma Processes
and Polymers

on the other hand, growing film oxidation with O$_2$ is negligible,[32,44] the appearance of the maximum with P_{RF} is attributed to an increase of atomic oxygen density, n_O. For these systems, the maximum nearly reaches the value of X_{FC}. This highlights the possibility to prepare oxide films using a target in the metallic state. Thus, higher ionization of the discharge allows modification of the chemical mechanisms in order to promote oxidation reaction on the growing films. After poisoning, when X_{Target} stabilizes (region 3), for Ti-Ar/O$_2$ and Ag-Ar/O$_2$, $O_{2,ads}$ shows no dependence on P_{RF}. On the contrary, for Sn-Ar/O$_2$, $O_{2,ads}$ decreases with P_{RF} (especially between $P_{RF} = 0$ and 100 W) due to the modification of X_{Plasma} with P_{RF} (Figure 7).

Finally to emphasize the possible technical improvement thanks to the use of iRMS processes, Figure 12 presents, for Sn-Ar/O$_2$, the evolutions of R_D and X_{Films} for $P_{RF} = 0$ and 200 W. When using iRMS plasma, X_{FC} is reached for $p_{O2,in} \approx 0.5$ mTorr while $p_{O2,in} \approx 3$ mTorr for conventional discharges. This modification allows to prepare fully stoichiometric films keeping the target in the metallic mode (arrows on Figure 12). Consequently, for a given X_{Films}, R_D increases by approximately a factor 6 (Table 4). The same reasoning for Ag-Ar/O$_2$ leads to an increase of about 25% of R_D. In the case of Ti-Ar/O$_2$, since the use of iRMS discharge does not affect the plasma nor the film compositions, this effect is not observed.

Conclusion

The goal of this work was to experimentally study the chemical mechanisms occurring during RMS. The three main parts of the RMS process (target, plasma and substrate) are monitored by both electrical and deposition rate, MS and XPS measurements, respectively. By studying reactive sputtering of Sn, Ag and Ti in Ar/O$_2$ mixture for conventional and RF coil iRMS discharges; it has been possible to interpret the different behaviors of these systems in terms of metal reactivity towards O$_2$.

By assessing target surface (by discharge voltage, V_D and deposition rate, R_D measurements) and plasma (by MS) chemistries, it is highlighted, on the one hand, that target poisoning occurs by reactive ions implantation and is not influenced by using iRMS discharges and, on the other hand, that target surface chemistry depends on plasma amplification by modifying chemisorptions of atomic oxygen on the substrate surface. The latter effect is particularly evident for Sn.

The consumption of O$_2$ by RMS process was measured using RGA. It is found to be dependent on metal reactivity to O$_2$ and plasma amplification. The significant increase of O$_2$ consumption in iRMS discharge is mainly related to the improvement of O$_2$ dissociation.

It is demonstrated that adsorption of reactive species by the growing films, depicted by the parameter k_{ox} calculated from XPS results, depends also on both the metal reactivity and plasma amplification. k_{ox} shows no dependence on plasma amplification for Ti-Ar/O$_2$, increases linearly for Sn-Ar/O$_2$ and increases up to a stable value for Ag-Ar/O$_2$.

Considering that metal oxide film synthesis involves two simultaneous mechanisms, namely condensation of sputtered compound and oxidation of the growing film by reactive species present in the discharge (O, O$_2$), it appears that the relative importance of these mechanisms depends on the metal reactivity and on the atomic oxygen density.

The striking influence of plasma amplification occurs before target poisoning. In this region it is possible, by using iRMS discharge, to promote reactions at the substrate for Sn-Ar/O$_2$ and Ag-Ar/O$_2$. Such modifications of the synthesis mechanisms allow deposition of tin and silver oxide films keeping the target in the metallic mode. In these conditions, the deposition rates are 6 times and 25% higher for Sn-Ar/O$_2$ and Ag-Ar/O$_2$, respectively, when compared to conventional RMS.

Nomenclature

X_{Target}:	Target surface composition
X_{Plasma}:	Plasma composition
X_{Film}:	Film composition
R_D:	Deposition rate
V_D:	Target voltage
I_D:	Target current
I_d:	Target current density
P_{RF}:	RF power applied to the coil
n_e:	Electron density
T_e:	Electron temperature
γ:	Secondary electron emission coefficient
p_{tot}:	Discharge pressure
p_R	Partial pressure of reactive gas R
Φ_R:	Inflow rate of reactive gas R
$\Phi_{R,c}$:	Critical inflow rate of reactive gas R when poisoning occurs
Φ_{Tot}:	Total inflow rate (Ar + O$_2$)
Φ_{O2}:	Inflow rate of O$_2$
Φ_{Ar}:	Inflow rate of Ar
f_{O2}:	Fraction of O$_2$ in the gas mixture
$p_{O2,in}$:	Input partial pressure of O$_2$
$p_{O2,eff}$:	Effective partial pressure of O$_2$
n_O:	Atomic oxygen density
ξ_M:	Metal reactivity to oxygen
$O_{2,cons}$:	Input O$_2$ consumed by the process
x_M:	Molar fraction of metal present in the plasma
X_{FC}:	Full stoichiometry of the film

k_{ox}:   Reactive species-growing film reaction parameter

α_i^j: Reaction coefficient between reactive gas species and growing film

$O_{2,ads}$: O_2 incorporated by adsorption reaction on the growing films

[1] N. Vershinin, K. Filonov, B. Straumal, W. Gust, I. Wiener, E. Rabkin, A. Kazakevich, *Surf. Coat. Technol.* **2000**, *125,* 229.
[2] K. L. Dham, P. A. Dearnley, *Wear* **2005**, *259,* 933.
[3] *"Semiconducting Transparent Thin Films"*, H. L. Hartnagel, A. L. Dawar, A. K. Jain, C. Jagadish, IOP, Bristol 1995.
[4] C. Schaefer, G. Braeuer, J. Szczyrbowski, *Surf. Coat. Technol.* **1997**, *93,* 37.
[5] *"Reactive sputtering: introduction and general discussion, Handbook of thin solid film process technology"*, W. D. Westwood, IOP, Bristol 1998.
[6] S. Berg, T. Nyberg, *Thin Solid Films* **2005**, *476,* 215.
[7] J. Heller, *Thin Solid Films* **1973**, *17,* 163.
[8] T. Abe, T. Yamashina, *Thin Solid Films* **1975**, *30,* 19.
[9] A. H. Eltoukhy, B. R. Natarajan, J. E. Greene, T. L. Barr, *Thin Solid Films* **1980**, *63,* 229.
[10] G. Lemperière, J. M. Poitevin, *Thin Solid Films* **1984**, *111,* 339.
[11] S. Berg, H.-O. Blom, T. Larsson, C. J. Nender, *J. Vac. Sci. Technol. A* **1987**, *5,* 202.
[12] A. Erschov, L. Pekker, *Thin Solid Films* **1996**, *289,* 140.
[13] L. Pekker, *Thin Solid Films* **1998**, *312,* 341.
[14] D. Depla, R. de Gryse, *Surf. Coat. Technol.* **2004**, *183,* 184.
[15] J. Hopwood, F. Qian, *J. Appl. Phys.* **2004**, *95,* 1.
[16] J. Joo, *J. Vac. Sci. Technol. A* **2000**, *18,* 23.
[17] K. F. Chiu, Z. H. Barber, *J. Appl. Phys.* **2002**, *91,* 4.
[18] S. Konstantinidis, A. Ricard, M. Ganciu, J.-P. Dauchot, C. Ranea, M. Hecq, *J. Appl. Phys.* **2004**, *95,* 1.
[19] S. M. Rossnagel, J. Hopwood, *Appl. Phys. Lett.* **1995**, *78,* 758.
[20] *"Handbook of Chemistry and"*, 57th Edition, CRC Press, Cleveland 1977.
[21] *"Glow discharges processes"*, B. Chapman, Ed., Wiley, New York 1980.
[22] W. Trennepohl, J. Bretagne, G. Gousset, D. Pagnon, M. Touzeau, *Plasma Sources Sci. Technol.* **1996**, *5,* 607.
[23] N. Li, J. P. Allain, D. N. Ruzic, *Surf. Coat. Technol.* **2002**, *149,* 161.
[24] D. Mao, K. Tao, J. Hopwood, *J. Vac. Sci. Technol. A* **2002**, *20,* 379.
[25] K. Tao, D. Mao, J. Hopwood, *J. Appl. Phys.* **2002**, *91,* 4040.
[26] D. Mao, J. Hopwood, *J. Appl. Phys.* **2004**, *96,* 820.
[27] T. Nyberg, S. Berg, U. Helmersson, K. Kartig, *Appl. Phys. Lett.* **2005**, *86,* 16410.
[28] S. M. Rossnagel, J. J. Cuomo, W. D. Westwood, *"Handbook of plasma processing"*, Noyes, Park Ridge, NJ 1990; p. 233–257.
[29] *PPM 421 Handbook*, Balzers, Liechtenstein 1998.
[30] J. H. Scofield, *J. Electron Spectrosc. Relat. Phenom.* **1976**, *8,* 123.
[31] D. Depla, R. de Gryse, *Plasma Sources Sci. Technol.* **2001**, *10,* 547.
[32] R. Snyders, M. Wautelet, R. Gouttebaron, J. P. Dauchot, M. Hecq, *Thin Solid Films* **2003**, *423,* 125.
[33] R. Mientus, K. Ellmer, *Surf. Coat. Technol.* **1999**, *116,* 1093.
[34] D. Depla, R. de Gryse, *Vacuum* **2003**, *69,* 529.
[35] D. Depla, J. Heamers, R. de Gryse, *Plasma Sources Sci. Technol.* **2002**, *11,* 91.
[36] D. Depla, R. de Gryse, *Surf. Coat. Technol.* **2004**, *183,* 184.
[37] D. Depla, R. de Gryse, *Surf. Coat. Technol.* **2004**, *183,* 190.
[38] D. Depla, R. de Gryse, *Surf. Coat. Technol.* **2004**, *183,* 196.
[39] D. Depla, D. Güttler, B. Abenroth, R. Gröztzchel, W. Möller, *Appl. Phys. Lett.* **2004**, *85,* 6134.
[40] D. Depla, R. de Gryse, *J. Vac. Sci. Technol. A* **2002**, *20,* 521.
[41] M. Kaminsky, *"Atomic and Ion Impact Phenomena on Metal Surfaces"*, Springer, Berlin 1965.
[42] R. Snyders, R. Gouttebaron, J. P. Dauchot, M. Hecq, *J. Vac. Sci. Technol. A* **2004**, *22,* 1540.
[43] R. Snyders, R. Gouttebaron, J. P. Dauchot, M. Hecq, *Surf. Coat. Technol.* **2005**, *200,* 448.
[44] R. Snyders, M. Wautelet, R. Gouttebaron, J. P. Dauchot, M. Hecq, *J. Anal. At. Spectrom.* **2003**, *18,* 618.
[45] R. Snyders, R. Gouttebaron, J. P. Dauchot, M. Hecq, *J. Vac. Sci. Technol. A* **2004**, *22,* 1540.
[46] R. Snyders, M. Wautelet, R. Gouttebaron, J. P. Dauchot, M. Hecq, *J. Anal. At. Spectrom.* **2003**, *18,* 618.
[47] J. M. Andersson, E. Wallin, E. P. Münger, U. Helmersson, *Appl. Phys. Lett.* **2006**, *88,* 054101.
[48] J. W. Coburn, E. Taglauer, E. Kay, *Jpn. J. Appl. Phys. Suppl.* **1974**, *2,* 501.
[49] F. Honda, G. M. Lancaster, Y. Fukuda, J. W. Rabalais, *J. Chem. Phys.* **1978**, *69,* 4931.
[50] B. J. Garrrison, N. Winograd, D. E. Harrison, Jr., *Phys. Rev. B: Condens. Matter* **1978**, *18,* 6000.
[51] R. Nyholm, N. J. Martensseon, *Phys. Chem.* **1980**, *13,* L279.
[52] R. Gouttebaron, D. Cornelissen, R. Snyders, J. P. Dauchot, M. Wautelet, M. Hecq, *Surf. Interface Anal.* **2000**, *30,* 527.
[53] S. W. Gaarenstroom, N. J. Winograd, *Chem. Phys.* **1977**, *67,* 3500.
[54] S. Konstantinidis, A. Ricard, R. Snyders, H. Vandeparre, J. P. Dauchot, M. Hecq, *Surf. Coat. Technol.* **2005**, *200,* 841.